The size correction without the z.p.e. terms is shown in Fig. 2. The curves in Fig. 1 and Fig. 2 coincide at high temperatures because the z.p.e. terms are relatively unimportant. As the temperature decreases the correction without z.p.e. terms (Fig. 2) increases, because the thermal contribution of the surface terms increases relative to the volume terms. This follows from the frequency distribution $g(\nu)$ in which the volume term is proportional to ν^2 and the surface term proportional to ν. On further lowering of the temperature the correction falls to zero since at these very low temperatures long wavelength modes which are possible in the large particles cannot exist in the small particle.

The influence of γ on the resulting curves is small. This is seen from Fig. 1, where the broken line is for $\gamma=0{\cdot}923$ whilst the other lines are for $\gamma=0{\cdot}973$. In the other Figures $\gamma=0{\cdot}973$.

For thin films the thickness correction is qualitatively similar to that for cubical particles as may be seen from Fig. 3. These curves include the B' terms which are the contributions of the low frequency modes omitted in the integrals. Because B' has been calculated with a thickness to length ratio of 10^{-3}, the curves are not as general as those for cubes. In particular this is the case for $N_z=10$ and 33·3. For the thicker films the influence of B' is small.

As expected, the correction for films is smaller than that for cubes with an edge length equal to the film thickness. At high temperatures it is somewhat larger than $\frac{1}{3}$ of that for cubes. The correction without z.p.e. terms for films is uncertain for low temperatures. At high temperatures it is the same as that which includes the z.p.e. terms. As the temperature decreases it first increases and then decreases in a manner which is qualitatively similar to that for cubes.

The author would like to thank Dr L. A. Vermeulen for frequent discussions and for reading the manuscript.

References

BOLT, R. H. (1939). *J. Acoust. Soc. Amer.* **10**, 228.
LOVE, A. E. H. (1944). *Mathematical Theory of Elasticity*. New York: Dover Publications.
MAA, D. Y. (1939). *J. Acoust. Soc. Amer.* **10**, 235.
MARSHALL, S. W. & WILENZICK, R. M. (1966). *Phys. Rev. Letters*, **16**, 219.
MONTROLL, E. W. (1950). *J. Chem. Phys.* **18**, 183.
ROE, G. M. (1941). *J. Acoust. Soc. Amer.* **13**, 1.
SOMMERFELD, A. (1945). *Mechanik der deformierbaren Medien*. Leipzig: Akademische Verlagsgesellschaft.
THIEL, R. C. (1967). *Z. Phys.* **200**, 227.
TOLSTOY, I. & USIDIN, E. (1953). *Geophysics*, **28**, 844.

Acta Cryst. (1968). A**24**, 619

The Resolution Function in Neutron Diffractometry. III. Experimental Determination and Properties of the 'Elastic Two-Crystal' Resolution Function*

BY M. J. COOPER†
Materials Physics Division, A.E.R.E., Harwell, Berkshire, England

AND R. NATHANS
Brookhaven National Laboratory, Upton, N.Y. 11973, *U.S.A.*

(*Received* 6 *June* 1968)

The experimental determination of the resolution function of a two-crystal neutron diffractometer is discussed. The form of the Bragg reflexion profiles observed for a perfect crystal using conventional scanning modes is considered in detail and their application to the measurement of diffuse elastic scattering is discussed.

1. Introduction

In earlier papers we have discussed the derivations of the resolution function for a three-crystal neutron diffractometer (paper I; Cooper & Nathans, 1967) and for a two-crystal neutron diffractometer for elastic scattering (paper II; Cooper & Nathans, 1968) in terms of a matrix notation involving the parameters of the system.

Although the matrix formulation is convenient for calculating the resolution function for a particular set of Gaussian instrumental parameters, it does not give us any direct or simple indication of the form of the dependence of the resolution function on the various parameters, and the extraction of this information from the matrix elements becomes complex. In addition it does not give us a clear indication of how well we can

* Work performed in part under the auspices of the U.S. Atomic Energy Commission.

† Formerly Research Associate, Brookhaven National Laboratory, Upton, N.Y , U.S.A.

determine the resolution function experimentally. For these reasons we shall consider in detail the form of Bragg reflexion profiles observed for a perfect crystal using the conventional scanning modes of a two-crystal diffractometer, which enables us to calculate the probability function at any point in reciprocal space. The resolution function can be determined experimentally by the measurement of such profiles and we shall discuss the application of the resolution function to the measurement of diffuse scattering.

2. Measurement of a Bragg reflexion from a perfect crystal

As we pointed out in paper I, the resolution function can be determined experimentally by scanning through a Bragg reflexion from a perfect crystal and in the case of a two-crystal diffractometer it is only the dependence on the component of $\Delta\mathbf{Q}||\mathbf{Q}$ that we cannot determine exactly in this way. However, we will show that a correction can be made if necessary.

We shall use the same notation as before and define divergence angles and mosaic and collimation parameters as before (see papers I and II).

If the Bragg angle for the sample is θ_B, then the Bragg condition is given by:

$$2\theta_S = 2\theta_B \tag{1a}$$

and

$$\Delta\mathbf{Q} = \Delta\mathbf{k}_i - \Delta\mathbf{k}_f = 0\,. \tag{1b}$$

We can then derive the dependence of Δk_i, γ_2' and δ_2' on γ_1' and δ_1' (the Bragg constraint) where γ' and δ' are the horizontal and vertical divergence angles with reference to the optimum paths for Bragg reflexion, and subscripts 1 and 2 refer to monochromator-to-sample and sample-to-detector regions respectively. We can then integrate over γ_1 and δ_1 for any general position to give the value of the resolution function at the Bragg reciprocal lattice point. In the Appendix to the present paper we derive the Bragg constraint and carry out the integration for points on crystal angle, detector angle and compound scans. The intensity profiles predicted for these scans are, as expected, Gaussian and the value of the resolution function at any point can be calculated from the expression for the appropriate scan. Contours of constant probability are ellipsoids and the orientation of these ellipsoids is also derived in the Appendix. In a later paper (paper IV, Cooper, 1968) we shall consider in detail the dependence of profiles measured with crystal angle (φ) and θ–2θ scans, on the instrumental parameters and extend the analysis to the case of finite mosaic spread in the sample.

3. Features of the resolution function

The form of the resolution function can best be illustrated by considering the locus of points at which the function has a given value, for example the resolution ellipsoid for which the probability is 50% (of R_0). The $\Delta\mathbf{Q}_z = 0$ section of such an ellipsoid is shown in Fig. 1 for a typical experimental arrangement. The section of the locus of 50% probability for neutrons in the monochromatized beam is also shown. This is also an ellipse and it can be shown that the angle μ_1 between the longer principal axis and $\mathbf{k}_I$ is given by the expression

$$\tan 2\mu_1 = \frac{2\tan\theta_M\left(\frac{1}{\eta_M^2}+\frac{2}{\alpha_0^2}\right)}{\left(\frac{1}{\eta_M^2}+\frac{1}{\alpha_0^2}+\frac{1}{\alpha_1^2}\right)-\left(\frac{1}{\eta_M^2}+\frac{4}{\alpha_0^2}\right)\tan^2\theta_M}\,. \tag{2}$$

For the case of relaxed in-pile collimation, $\alpha_0 \gg \eta_M$, this reduces to

$$\tan 2\mu_1 = \frac{2\tan\theta_M}{1+\frac{\eta_M^2}{\alpha_1^2}-\tan^2\theta_M}\,. \tag{3}$$

If the monochromator to sample collimation is also relaxed, $\alpha_1 \gg \eta_m$, this then gives

$$\tan 2\mu_1 \simeq \tan 2\theta_m\,. \tag{4}$$

Hence for completely relaxed collimation $\mu_1 = \theta_m$ and μ_1 decreases as α_1/η_m becomes smaller.

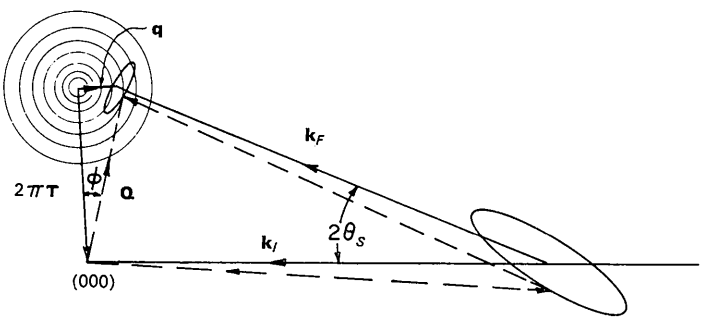

Fig. 1. Sketch of reciprocal space showing the effects of finite collimation and mosaic spread in the monochromator. The larger ellipse represents the termination of the wave vectors of the monochromated neutrons, with 50% of the maximum probability; the smaller ellipse represents the termination of the scattering vectors with 50% of the maximum probability (the resolution ellipse). The concentric circles represent contours of constant $|q|$ about a reciprocal lattice point.

The shape of the resolution ellipsoid will depend on the value of θ_S. One principal axis of the horizontal ellipse ($\Delta Q_z=0$) will be directed towards **Q** and the angle μ_2 between these directions is derived in the Appendix (equation 50). However, the magnitude of the two principal axes in this plane will depend on θ_S, such that at low values the resolution ellipsoid becomes disc-like in shape with the plane of the disc lying towards **Q** and ΔQ_z. As θ_S increases, the horizontal ellipse becomes more circular and then at high values of θ_S becomes elongated and roughly perpendicular to **Q**. This change in shape arises mainly from geometrical considerations. An example of the type of curve found at low angles is shown in Fig. 2. This is a central horizontal section ($\Delta Q_z=0$) of the resolution function obtained experimentally for the magnetic $\frac{1}{2}\frac{1}{2}\frac{1}{2}$ reflexion of $KMnF_3$ ($\theta_S\sim 6°$), using a series of φ and 2θ scans, and shows a number of probability contours of equal interval.

4. Application to diffuse scattering

It may be seen that the shape of the resolution function can be exploited in the measurement of diffuse scattering by choosing a type of scan for which it is most favourable. For example, in Fig. 1, we show contours for critical magnetic scattering about a point in reciprocal space and at small values of θ_S a crystal φ-scan, in which the crystal is rotated and the detector remains stationary, is clearly most advantageous since the resolution function will then traverse the reciprocal lattice point most rapidly, leading to the least distortion of the peak shape. (This is analogous to the mode of scan focusing for inelastic phonon peaks discussed in paper I.) This type of scan also has the advantage that since $2\theta_S$ is fixed, the resolution is not varying during the scan.

Since we are considering only the case of elastic scattering it is in theory always possible to determine the true resolution function of the diffractometer experimentally, subject to the approximation in the $2\theta_S$ dependence, whenever a perfect Bragg reflexion is available at the appropriate scattering angle. In this case the theoretical intensity can be calculated directly from the cross section by numerical integration without invoking any Gaussian approximations. For a perfect crystal sample we have:

$$I(\mathbf{Q}_0)=\int R(\mathbf{Q}_0+\Delta\mathbf{Q})\sigma(\mathbf{Q}_0+\Delta\mathbf{Q})\Delta\mathbf{Q}\,. \qquad (5)$$

However, for a sample with finite mosaic spread we must first integrate the cross section over the mosaic spread, $M(\mathbf{q}_m)$, where $\mathbf{q}_m$ is the reciprocal lattice vector defining translation from the point of optimum Bragg reflexion (see equations (6) and (7) of paper II).

$$I(\mathbf{Q}_0)=\int\left\{\int\sigma(\mathbf{Q}_0+\Delta\mathbf{Q}+\mathbf{q}_m)\times M(\mathbf{q}_m)\mathbf{dq}_m\right\}R(\mathbf{Q}_0+\Delta\mathbf{Q})\Delta\mathbf{Q}\,. \qquad (6)$$

Similarly the resolution function determined using a Bragg reflexion from a sample with mosaic spread $M'(\mathbf{q}_m)$ is given by:

$$R'(\mathbf{Q}_0+\Delta\mathbf{Q})=\int M'(\mathbf{q}_m)R(\mathbf{Q}_0+\Delta\mathbf{Q}+\mathbf{q}_m)\mathbf{dq}_m\,. \qquad (7)$$

The resolution function should therefore be determined using a crystal with as small a mosaic spread as possible and with a Bragg reflexion having a 2θ value as close as possible to that for which the true resolution function is required.

If the sample itself has a Bragg reflexion at the required angle, as for example in the case of critical magnetic scattering from an antiferromagnet (Cooper & Nathans, 1966), then this reflexion may be used to determine the resolution function directly. In this case $M'(\mathbf{q}_m)=M(\mathbf{q}_m)$ and if this mosaic spread is small we may be justified in using the approximation for equation (6):

$$I(\mathbf{Q}_0)=\int\sigma(\mathbf{Q}_0+\Delta\mathbf{Q})R'(\mathbf{Q}_0+\Delta\mathbf{Q})\Delta\mathbf{Q}\,, \qquad (8)$$

thus avoiding the necessity for unfolding the mosaic from the observed function.

It should be emphasized that under these conditions the true experimental resolution function can be used whatever its form, and the theory using Gaussian approximations is required only for the calculation of the resolution function at different scattering angles. The theoretical intensity can then be calculated from equations (6) or (8) for any scattering cross-section and compared directly with the corresponding observed intensity.

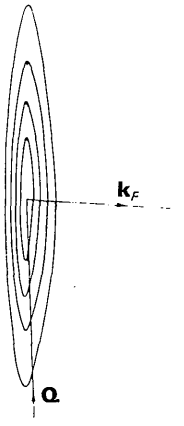

Fig. 2. $\Delta Q_z=0$ section of an experimentally determined resolution function for $KMnF_3$, showing loci of equal probability at intervals of $0{\cdot}2P_{max}$.

APPENDIX
The Bragg constraint

The derivation of the Bragg constraint has been outlined above. If we consider $2\theta_S=2\theta_B$ and equate the

components of **ΔQ** to zero we obtain from equations (11) of paper II

$$-x_1 2\sin\theta_B+(y_2'-y_1')\cos\theta_B=0 \qquad (9a)$$

$$(y_2'+y_1')\sin\theta_B=0 \qquad (9b)$$

$$z_2'-z_1'=0 \qquad (9c)$$

where y' and z' are defined in terms of the divergence angles γ' and δ' with reference to the optimum paths for Bragg reflexion, *e.g.* $y_1'=\gamma_1' k_I$.

Hence the Bragg constraint is:

$$x_1=-y_1'\cot\theta_B \qquad (10a)$$

$$y_2'=-y_1' \qquad (10b)$$

$$z_2'=z_1'\,. \qquad (10c)$$

For any given setting we can relate the divergence angles for the collimators to γ' and δ'. The value of the resolution function is then given by

$$R=R_H\times R_V$$

$$=\int_{-\infty}^{\infty}P_H(\Delta k_i,\gamma_1,\gamma_2)\,\mathrm{d}y_1\int_{-\infty}^{\infty}P_V(\delta_1,\delta_2)\mathrm{d}z_1 \qquad (11)$$

where the first integration is carried out subject to the Bragg constraint, and from paper II, equation (3) we have

$$P_H=P_M P_0\exp\left\{-\frac{1}{2}\left[\left(\frac{(\Delta k_i/k_I)\tan\theta_M+\gamma_1}{\eta_M}\right)^2+\left(\frac{2(\Delta k_i/k_I)\tan\theta_M+\gamma_1}{\alpha_0}\right)^2+\frac{\gamma_1^2}{\alpha_1^2}+\frac{\gamma_2^2}{\alpha_2^2}\right]\right\} \qquad (12)$$

$$P_V=\exp\left\{-\frac{1}{2}\left[\left(\frac{\delta_1^2}{4\tan^2\theta_M\eta_M'^2+\beta_0^2}\right)+\frac{\delta_1^2}{\beta_1^2}+\frac{\delta_2^2}{\beta_2^2}\right]\right\}. \qquad (13)$$

Table 1. *Definitions*

A_j	$=1/(\alpha_k k_I)$	for $j=0,1,2$
B^2_0	$=1/(Q^2_M\eta'^2_M+\beta^2_0 k^2_I)$	
B_j	$=1/(\beta_j k_I)$	for $j=1,2$
C_0	$=A_0(2\cot\theta_B\tan\theta_M-1)$	
C_1	$=H_M(\cot\theta_B\tan\theta_M-1)$	
D^2_H	$=C^2_0+C^2_1+A^2_1+A^2_2$	
D^2_V	$=B^2_0+B^2_1+B^2_2$	
E_H	$=k_I(H_M C_1-A_0C_0-A^2_1+A^2_2)/D_H$	
F^2_H	$=k^2_I(H^2_M+A^2_0+A^2_1+A^2_2)-E^2_H$	
G	$=Q(B^2_0+B^2_1-B^2_2)/(2D_V)$	
H_M	$=1/(\eta_M k_I)$	
J^2	$=Q^2(B^2_0+B^2_1)B^2_2/D^2_V$	
$K_{\varphi,2\theta}$	$=E_H\varphi-L\Delta 2\theta$	
L	$=k_I A^2_2/D_H$	
L_S	$=k^2_I A^2_2(C^2_0-A_0C_0+C^2_1-H_MC_1+2A^2_1)/D^2_H$	
N^2	$=k^2_I(C^2_0+C^2_1+A^2_1)A^2_2/D^2_H$	
R_0	$=2\pi P_M P_0/(D_H D_V)$	
$S^2_{\varphi,2\theta}$	$=F^2_H\varphi^2+N^2(\Delta 2\theta)^2-2\varphi\Delta\theta L_S$	
$S^2_{\theta,2\theta}$	$=S^2_H(\Delta\theta)^2$	
S^2_H	$=F^2_H+4N^2-4L_S$	
T	$=L_S/F_H$	

Intensity under optimum Bragg conditions

For the case where $2\theta_S=2\theta_B$ and the sample is set to give the optimum intensity, the divergence angles γ' and δ' will be the true divergence angles for the collimators, *i.e.* $\gamma=\gamma'$, $\delta=\delta'$.

The notation used in the following sections is summarized in Table 1. It is convenient to write:

$$\frac{1}{\eta_M k_I}=H_M \qquad \frac{1}{\alpha_j k_I}=A_j\ (j=0,1,2)$$

$$\frac{1}{Q^2_M\eta'^2_M+\beta^2_0 k^2_I}=B^2_0 \qquad \frac{1}{\beta_j k_I}=B_j\ (j=1,2) \qquad (14)$$

Then from equations (10) and (12) we have

$$P_H=P_M P_0\exp\{-\tfrac{1}{2}[H^2_M(y_1'\cot\theta_B\tan\theta_M-y_1')^2+A^2_1 y_1'^2+A^2_2 y_1'^2+A^2_0(y_1'^2\cot\theta_B\tan\theta_M-y_1')^2]\} \qquad (15)$$

$$=P_M P_0\exp\{-\tfrac{1}{2}D^2_H y_1'^2\} \qquad (16)$$

where

$$D^2_H=C^2_0+C^2_1+A^2_1+A^2_2 \qquad (17a)$$

$$C_0=A_0(2\cot\theta_B\tan\theta_M-1) \qquad (17b)$$

$$C_1=H_M(\cot\theta_B\tan\theta_M-1)\,. \qquad (17c)$$

The resolution function is then given from equation (11) by:

$$R_0=P_M P_0\int_{-\infty}^{\infty}\exp\{-\tfrac{1}{2}D^2_H y_1'^2\}\mathrm{d}y_1'\times\int_{-8}^{\infty}\exp\{-\tfrac{1}{2}(B^2_0+B^2_1+B^2_2)z_1'^2\}\mathrm{d}z_1' \qquad (18)$$

$$=\frac{2\pi P_M P_0}{D_H D_V} \qquad (19)$$

where

$$D^2_V=B^2_0+B^2_1+B^2_2\,. \qquad (20)$$

The intensity I_0 is then proportional to R_0.

Horizontal crystal (φ) scan

If we now rotate the crystal about a vertical axis, through an angle φ from the optimum position, the measured intensity will be reduced.

We can introduce the Bragg constraints as before. However, the optimum directions will be rotated through an angle φ so that we have the relations:

$$\gamma_1=\gamma_1'-\varphi \quad \gamma_2=\gamma_2'-\theta \qquad (21)$$

giving

$$P_H=P_M P_0\exp\{-\tfrac{1}{2}[H^2_M[(\cot\theta_B\tan\theta_M-1)y_1'+\varphi k_I]^2+A^2_1(y_1'-\varphi k_I)^2+A^2_2(y_1'+\varphi k_I)^2+A^2_0[(2\cot\theta_B\tan\theta_M-1)y_1'+\varphi k_I]^2]\} \qquad (22)$$

$$= P_M P_0 \exp\{-\tfrac{1}{2}[(D_H y_1' + E_H\varphi)^2 + F_H^2\varphi^2]\} \quad (23)$$

where

$$E_H = k_I(H_M C_1 + A_0 C_0 - A_1^2 + A_2^2)/D_H \quad (24a)$$

$$F_H^2 = k_I^2(H_M^2 + A_0^2 + A_1^2 + A_2^2) - E_H^2 . \quad (24b)$$

Integration over dy_1', dz_1' then gives

$$I_\varphi = I_0 \exp\{-\tfrac{1}{2}F_H^2\varphi^2\} . \quad (25)$$

Hence I_φ is a Gaussian function of φ with characteristic width $1/F_H$.

Vertical crystal (ψ) scan

If the crystal is rotated about a horizontal axis perpendicular to the scattering vector, through an angle ψ, we have the relations:

$$\delta_1 = \delta_1' - \frac{Q}{2k_I}\psi \qquad \delta_2 = \delta_2' + \frac{Q}{2k_I}\psi \quad (26)$$

so that

$$P_V = \exp\{-\tfrac{1}{2}[(B_0^2 + B_1^2)(z_1' - \tfrac{1}{2}Q\psi)^2 + B_2^2(z_1' + \tfrac{1}{2}Q\psi)^2]\} \quad (27)$$

$$= \exp\{-\tfrac{1}{2}[(D_V z_1' - G\psi)^2 + J^2\psi^2]\} \quad (28)$$

where D_V is defined by equation (20),

$$G = Q(B_0^2 + B_1^2 - B_2^2)/(2D_V) \quad (29a)$$

and

$$J^2 = \frac{Q^2(B_0^2 + B_1^2)B_2^2}{B_0^2 + B_1^2 + B_2^2} . \quad (29b)$$

Integration over dy_1', dz_1' then gives

$$I_\psi = I_0 \exp\{-\tfrac{1}{2}J^2\psi^2\} . \quad (30)$$

Hence I_ψ is a Gaussian function of ψ with characteristic width $1/J$.

Detector (2θ) scan

If we keep the crystal fixed and rotate the detector through an angle $\Delta 2\theta$ we have the relations

$$\gamma_1 = \gamma_1' \qquad \gamma_2 = \gamma_2' + k_I \Delta 2\theta \quad (31)$$

so that

$$P_H = P_M P_0 \exp\{-\tfrac{1}{2}[(C_0^2 + C_1^2 + A_1^2)y_1'^2 + A_2^2(y_1' - k_I\Delta 2\theta)^2]\} \quad (32)$$

$$= P_M P_0 \exp\{-\tfrac{1}{2}[(D_H y_1' - L\Delta 2\theta)^2 + N^2(\Delta 2\theta)^2]\} \quad (33)$$

where

$$L = k_I A_2^2/D_H \quad (34a)$$

$$N^2 = \frac{k_I^2(C_0^2 + C_1^2 + A_1^2)A_2^2}{C_0^2 + C_1^2 + A_1^2 + A_2^2} \quad (34b)$$

and C_0, C_1 and D_H are defined by equations (17).

Integration over dy_1', dz_1' then gives

$$I_{2\theta} = I_0 \exp\{-\tfrac{1}{2}N^2(\Delta 2\theta)^2\} \quad (35)$$

which is a Gaussian function of $\Delta 2\theta$ with characteristic width $1/N$.

As stated previously this type of scan will not measure the true resolution function, which would be given by keeping the detector fixed and moving the Bragg reflexion in reciprocal space. To arrive at an equivalent position we should have to move the detector through an arc of $-k_I\Delta 2\theta$, *i.e.* the new scattering angle would be $2\theta_S - \Delta 2\theta$. The above analysis would still be correct except that C_0 and C_1 would then be a function of $\Delta 2\theta$, namely

$$C_0 = A_0[2\cot(\theta_S - \tfrac{1}{2}\Delta 2\theta)\tan\theta_M - 1] \quad (36a)$$

$$C_1 = H_M[\cot(\theta_S - \tfrac{1}{2}\Delta 2\theta)\tan\theta_M - 1] . \quad (36b)$$

Hence the approximation involved in measuring the resolution function using a detector scan will depend on the range of $\Delta 2\theta$ and the relation between θ_S and θ_M.

General position (φ,ψ, 2θ)

Since the vertical and horizontal terms are independent, the ψ dependence is given simply by equation (30).

For the horizontal term we have

$$\gamma_1 = \gamma_2' - \varphi k_I \quad (37a)$$

$$\gamma_2 = \gamma_2' - (\varphi - \Delta 2\theta)k_I . \quad (37b)$$

Hence

$$P_H = P_M P_0\{-\tfrac{1}{2}[H_M^2[(\cot\theta_B\tan\theta_M - 1)y_1'^2 + \varphi k_I]^2 + (y_1' - \varphi k_I)^2 A_1^2 + (y_1' + \varphi k_I - \Delta 2\theta k_I)^2 A_2^2 + A_0^2[(2\cot\theta_B\tan\theta_M - 1)y_1' + \varphi k_I]^2]\} \quad (38)$$

$$= P_M P_0 \exp\{-\tfrac{1}{2}[(D_H y_1' + K_{\varphi,2\theta})^2 + S_{\varphi,2\theta}^2]\} \quad (39)$$

where

$$K_{\varphi,2\theta} = E_H\varphi - L\Delta 2\theta \quad (40a)$$

$$S_{\varphi,2\theta}^2 = F_H^2\varphi^2 + N^2(\Delta 2\theta)^2 - 2\varphi\Delta\theta L_S \quad (40b)$$

and

$$L_S = k_I^2 A_2^2(C_0^2 - A_0 C_0 + C_1^2 - H_M C_1 + 2A_1^2)/D_H^2 . \quad (40c)$$

D_H, E_H, F_H, L and N are defined in equations (17), (24) and (34). Integration over dy_1', dz_1' therefore gives

$$I_{\varphi,\psi,2\theta} = I_0 \exp\{-\tfrac{1}{2}S_{\varphi,2\theta}^2\} \exp\{-\tfrac{1}{2}J^2\psi^2\} . \quad (41)$$

Let us now consider a φ scan at constant 2θ. We can write

$$S_{\varphi,2\theta}^2 = [F_H\varphi - T(\Delta 2\theta)]^2 + (N^2 - T^2)(\Delta 2\theta)^2 \quad (42)$$

where

$$T = L_S/F_H . \quad (43)$$

The intensity is therefore proportional to

$$\exp\{-\tfrac{1}{2}[F_H\varphi - T(\Delta 2\theta)]^2\} \exp\{-\tfrac{1}{2}(N^2 - T^2)(\Delta 2\theta)^2\} \quad (44)$$

which is a Gaussian function of φ with a characteristic width $1/F_H$ and a maximum at $\varphi=\frac{T}{F_H}\Delta 2\theta$.

Similar results are obtained for a 2θ scan at constant φ.

θ–2θ Scan

For a θ–2θ scan, $\varphi=\Delta\theta$, so that from equation (40*b*) we have

$$S^2_{\theta,2\theta}=S^2_H(\Delta\theta)^2, \tag{45}$$

where

$$S^2_H=F^2_H+4N^2-4L_S\,. \tag{46}$$

The intensity is therefore given by

$$I_{\theta,2\theta}=I_0\exp\{-\tfrac{1}{2}S^2_H(\Delta\theta)^2\}, \tag{47}$$

which is a Gaussian function of $\Delta\theta$ with characteristic width $1/S_H$.

Orientation of the resolution ellipsoid

The results of the previous sections enable us to determine the size and orientation of the resolution ellipsoid. If we define orthogonal axes as before (paper II) with $\Delta\mathbf{Q}_x$ parallel to $\mathbf{Q}$ and $\Delta\mathbf{Q}_z$ vertical, we can derive the resolution ellipsoid from equations (25), (30), (35) and (47) to be:

$$a\Delta Q^2_x+b\Delta Q^2_y+c\Delta Q^2_z+2h\Delta Q_x\Delta Q_y=1 \tag{48}$$

where

$$a=S^2_H/\cos^2\theta_S \tag{49a}$$

$$b=F^2_H/\sin^2\theta_S \tag{49b}$$

$$c=J^2/\sin^2\theta_S \tag{49c}$$

$$h=(2L_S-F^2_H)/(\sin\theta_S\cos\theta_S) \tag{49d}$$

and the angles μ_2 made by the principal axes to $\mathbf{Q}$ are given by $\tan\mu_2=m_j$ ($j=1$, 2, or 3), where m_1 and m_2 are given by the roots of the equation

$$hm^2+m(a-b)-h=0 \tag{50}$$

and $m_3=\infty$.

References

COOPER, M. J. & NATHANS, R. (1966). *J. Appl. Phys.* **37** 1041.

COOPER, M. J. & NATHANS, R. (1967). *Acta Cryst.* **23**, 357.

COOPER, M. J. & NATHANS, R. (1968). *Acta Cryst.* A**24**, 481.

COOPER, M. J. (1968). A**24**, 624.

Acta Cryst. (1968). A**24**, 624

The Resolution Function in Neutron Diffractometry IV. Application of the Resolution Function to the Measurement of Bragg Peaks*

BY M. J. COOPER†

Materials Physics Division, A.E.R.E., Harwell, Berks., England

(*Received* 6 *June* 1968)

The application of the resolution function of a two-crystal neutron diffractometer to the measurement of Bragg peaks is discussed in detail and experimental measurements of peak widths are compared with theoretical predictions.

1. Introduction

In the previous paper (part III: Cooper & Nathans, 1968) we derived the form of various scans through a Bragg peak for a perfect crystal sample in order to demonstrate the use of experimental Bragg profile measurements in determining the resolution function of a two-crystal neutron diffractometer. In the present paper we shall examine more closely the dependence of these scans on the instrumental parameters, considering such factors as focusing effects, and extend the analysis to the case of Bragg peaks for imperfect single crystals. Experimental results which support this analysis are also given.

2. Crystal (φ) scans

(*a*) *Perfect sample*

The intensity observed when a perfect sample has been rotated through an angle φ from the optimum setting for the measurement of a Bragg reflexion has been derived in equation (25) of paper III. The characteristic width of a φ-scan is $\Phi_0=1/F_H$, where F_H is defined by equation (24*b*) of paper III.

* Work performed in part under the auspices of the U.S. Atomic Energy Commission.

† Formerly Research Associate, Brookhaven National Laboratory, N.Y., U.S.A.